ToF-SIMS analyses of brake wear particles in human epithelial Caco-2 cells

Journal of Aerosol Science 186 (2025) 106553

Contents lists available at ScienceDirect

Journal of Aerosol Science

journal homepage: www.elsevier.com/locate/jaerosci

ToF-SIMS analyses of brake wear particles in human epithelial Caco-2 cells

Robin Rydbergh [a], Lisa-Marie Witte [a], Jonas Sjöblom [b], Nathalie Scheers [a,*], Amir Saeid Mohammadi [c], Eric Voortman Landström [b], Tore V. Vernersson [b], Per Malmberg [d,**]

[a] Chalmers University of Technology, Department of Life Sciences, 41296, Gothenburg, Sweden
[b] Chalmers University of Technology, Department of Mechanics and Maritime Sciences, 41296, Gothenburg, Sweden
[c] Chalmers University of Technology, Department of Architecture and Civil Engineering, 41296, Gothenburg, Sweden
[d] Chalmers University of Technology, Department of Chemistry and Chemical Engineering, 41296, Gothenburg, Sweden

ARTICLE INFO

Handling editor: Chris Hogan

Keywords:
Air pollution
Atmospheric particulate matter
PM2.5
HR-ELPI+
Caco-2
ToF-SIMS

ABSTRACT

Air pollutants, especially fine particulate matter (diameter of <2.5 μm), are associated with severe health risks including increased cardiopulmonary and lung cancer mortality and development of neurodegenerative diseases. This study introduces a novel methodology that begins with *in situ* particulate pollution collection, proceeds to exposing non-animal human epithelial cell models which are then analyzed through high spatial resolution mass spectrometry imaging to differentiate the chemistry of particles among exposed cells. During regular train operations, brake wear particles (BWP) are primarily generated from brake pad abrasion. For this work, a custom train brake rig was used to generate BWP, which were then introduced to human epithelial Caco-2 cells. First, the BWP size distributions were characterized using an Electrical Low-Pressure Impactor and particles ranging from 1.1 to 2.7 μm were collected with a gravimetric impactor. A suspension of these BWP, characterized by Dynamic Light Scattering, was added to Caco-2 cells cultured on coverslips. After incubation, the cells were washed and fixed by freeze-drying to preserve the epithelial structure. Subsequent analyses with SEM and Time-of-Flight Secondary Ion Mass Spectrometry (ToF-SIMS) established substantial, partially agglomerated, BWP deposits on the surface of the epithelial cellular structures. Further analysis of the ToF-SIMS data using Multivariate Curve Resolution-Alternating Least Squares, achieved a better separation of underlying chemical distributions. This enhanced image contrast facilitated the observation of particle-cell interactions. The results demonstrate the efficacy and potential of ToF-SIMS mass spectrometry imaging in distinguishing and potentially characterizing particle-cell interactions. This methodology may be further refined by incorporating complementary analytical techniques such as ICP-MS to better quantify metal content in particles and attempts with smaller particles might help assess cellular particle penetration and accumulation.

* Corresponding author.
** Corresponding author.
E-mail addresses: nathalie.scheers@chalmers.se (N. Scheers), per.malmberg@chalmers.se (P. Malmberg).

https://doi.org/10.1016/j.jaerosci.2025.106553
Received 28 May 2024; Received in revised form 28 January 2025; Accepted 24 February 2025
Available online 3 March 2025

1. Introduction

1.1. Air pollution and brake wear particles

Air pollution is a large environmental risk factor for adverse health effects and approximately 99% of the world's population breathes air that contains high levels of pollutants, leading to 6.8 million premature deaths annually (Ambient air pollution, 2022). Common sources of ambient air pollutants include both natural and anthropogenic emissions, the latter being caused by fossil fuel combustion, industrial activities, agriculture, and mining, amongst other sources (Maciejczyk et al., 2021). One of the main air pollutant constituents is particulate matter (PM), which is a diverse mixture of liquid and solid particles suspended in air, consisting of e.g. sulfates, nitrates, organic compounds and metals. Aerodynamic diameter is one of the main classification system for PM, the most common size categories being PM10 and PM2.5, with a particle diameter of less than 10 μm and 2.5 μm, respectively Click or tap here to enter text. PM2.5 is defined as fine PM, but also contains ultrafine particles (World Health Organization, 2013). According to the US Environmental Protection Agency (EPA), particles classified as PM2.5 pose the greatest risk to human health (Particulate Matter Basics, 2024).

Focusing on transport emissions, PM can be further divided into exhaust and non-exhaust emissions (NEE). Exhaust emissions are caused by incomplete fuel combustion processes, while NEE are the result of friction between material surfaces. The main causes of NEE are the wear of roads, tires and brakes from transport vehicles. This not only includes road transport, but also rail transport like trains, trams, or metro. Due to successively stricter fuel and tail-pipe emission standards, exhaust emissions have been decreasing in the last decades. However, NEE, which are not yet subject to similarly strict policies, are steadily increasing (Vanherle et al., 2021). Brake wear is the abrasion due to friction between the brake pad and its rotating disc or wheel, when forced together during the braking process. As a result of this abrasion, PM is emitted. The materials of the brake pad and disc influence the particle composition that is emitted during wear (Vanherle et al., 2021). Train brake pads can be made of several types of materials, the most common being cast iron, composite or sintered materials (Günay et al., 2020). Abbasi et al. (2012) collected and analyzed airborne brake wear particles (BWP) from a running regional train, resulting in considerable amounts of Fe, Cu, Zn, Ca, Mg, Al and Ni, while Fridell et al. (2011) found a correlation between mechanical braking and high particle emission from a running passenger train.

1.2. Susceptibility of respiratory passageways to air particles

The respiratory airways are lined with different types of cells with specialized functions. In the upper airways; the nasal cavity, pharynx and larynx, the epithelium heats and humidifies the incoming air (Jackson, 1996). The lower conducting airways, which include the trachea, bronchi, and bronchioles, direct the air further into the respiratory passageway. Alveoli in the respiratory zone facilitates gas exchange, in which O_2 and CO_2 are cycled between the lungs and the blood circulation (Davies & Moores, 2010). Immune cells infiltrated in the respiratory epithelium fight infections, while mucus-producing goblet cells neutralize pathogens and physically trap particles, e.g. pollutants, dust, pollen, bacteria, and viruses (Calvén et al., 2020). Other cell types in the epithelium cause protective respiratory reflexes such as sneezing, coughing and inhibition of breathing to avoid potential harm (Hewitt & Lloyd, 2021). This delicate system is affected by inhaled PM. Pollutant PM is deposited in the lungs after inhalation, by several mechanisms as reviewed by Darquenne (Darquenne, 2020) and in particular, PM2.5 is associated with health issues such as an increased risk of cardiopulmonary and lung cancer mortality (Hill et al., 2023; Pope III, 2002), cognitive dysfunction and Alzheimer's disease (Jung et al., 2015), as well as pregnancy complications and adverse birth outcomes (Song et al., 2023). In addition, the deposition of PM may lead to direct complications in the respiratory passageways such as asthma (McConnell et al., 2010), chronic pulmonary disease (Sarkar et al., 2019) and an increase the susceptibility of respiratory infections (Yang et al., 2020).

1.3. Analysis techniques to study cell particle interactions

When studying interactions between PM and biological systems there are some established approaches used for PM characterization which have already yielded insights towards the understanding of potential health effects of PM exposure. Such methods include TEM, XPS, FTIR, SEM and means of fluorescence microscopy among other techniques (Ivask et al., 2018; Mourdikoudis et al., 2018).

Time-of-Flight Secondary Ion Mass Spectrometry (ToF-SIMS) is an imaging mass spectrometry (MS) technique that utilizes a liquid metal ion cannon (LMIG) to shoot at a sample yielding bursts of secondary ions that are then collected in either positive or negative polarity in a time-of-flight mass analyzer. An LMIG can shoot at a sample in a precise 2D raster allowing for MS imaging where the spatial distributions of different molecular ion species can be compared and studied. This has already been done to some extent for studying synthetic silica and zirconia PM spatial distribution in biological systems. These studies used *in vivo* testing on rat lungs succeeding in demonstrating how the ToF-SIMS can chemically differentiate PM among biological matter (Veith et al., 2017, 2018).

ToF-SIMS imaging MS provides a unique ability to simultaneously identify and image the distribution particles, metals, and organic compounds. In addition, biological processes can be monitored since lipids and metabolites can be imaged and analyzed at the same time. TEM has a superior spatial resolution but lacks proper ability to chemically differentiate distribution of molecules. While XPS is great for chemically determining the surface of materials and could be used for imaging to some extent, ToF-SIMS can be used to gain a superior spatial resolution while maintaining the ability to chemically profile and differentiate the PM from biological matter. Additionally, XPS has a depth sensitivity that can be a challenge if the PM is internalized into cells and not accessible at the surface.

1.4. The present study

After inhalation, PM primarily deposits in the respiratory airways. However, PM can reach as far as the gastrointestinal tract, through mucociliary transport as well as ingestion and inhalation (Pambianchi et al., 2022). Therefore, deposition of PM in the gastrointestinal epithelium may also be of importance for PM exposure, since the first part of the airways and gastrointestinal tract are shared between the two. In the present study, the human intestinal epithelial Caco-2 cell model was used to study the deposition of PM. In a drug transport study, Tronde et al. (2003) showed that the apparent epithelial permeability of Caco-2 cell monolayers correlates with the apparent absorption rate of isolated, perfused and ventilated rat lung (IPL) models. There are many cell culture studies on PM and its epithelial and intracellular effects (Alfaro-Moreno et al., 2009; Upadhyay et al., 2022; Xu et al., 2019; Zhao et al., 2020) and a multitude of studies on the investigation of PM using ToF-SIMS (Huang et al., 2017; Peterson & Tyler, 2003; Zhu et al., 2001). Additionally, lung-nanoparticle interactions have been studied previously with ToF-SIMS (Najafinobar et al., 2019; Singh et al., 2020). In the present study, we aimed to develop a novel analytical approach to study PM deposition of μm size on epithelial cells to be able to follow the PM interaction using ToF-SIMS and Multivariate Curve Resolution-Alternating Least Squares (MCR-ALS).

2. Methods

2.1. Train brake test rig

The train brake tests were performed indoors using a novel brake test rig designed for research usage at the railway research center *Chalmers Railway Mechanics (CHARMEC)* at Chalmers University of Technology. The present brake tests have previously been reported with a focus on the thermomechanical behavior of wheels (Voortman Landström et al., 2024).

The train braking sequence is controlled using a custom LabVIEW script. Two SAB WABCO BFC tread brake units are mounted on free swinging arms and give the braking force by pressing the brake blocks towards the wheel tread. The brake blocks are mounted in a 2xBg configuration (single brake blocks on opposite sides of the wheel). The instantaneous power is calculated from measured torque (by a force transducer mounted to the arms) and rotational speed. The wheels are rotating at a constant speed of 60 km/h on the tread and the tests are each run at mean set power levels of between 20 and 50 kW for approximately 40 min.

The brake blocks are of the type Becorit 929–1, an organic composite brake block made of organic resin matrix and metal fibers with additives, designed for very high thermal loads. This type is not approved for general service use as it does not exhibit 'thermal fuse' capacity at higher temperatures, which is a requirement for protecting wheels from overheating, but it is widely used for braking tests in labs. Brake blocks intended for use in the field would show higher levels of particle emissions, in particular towards the higher end of the temperature range, above 500 °C. The brake blocks are bedded in to fit the wheel prior to the testing so that at least 80% of the brake shoe surface is in contact with the wheel (European Committee for Standardization, 2023). This measure is then improved throughout the continuous testing schedule as the blocks wear. The experimental brake rig setup is shown in Fig. 1.

2.2. Brake wear particle collection

Two parallel sampling lines from the brake rig were connected for BWP characterization and collection. Braking events were performed in similar conditions, with the major difference being changing brake power, with steps at every 5 kW between 20 and 50 kW. A more detailed explanation of the braking tests is given for wheel 3 in (Voortman Landström et al., 2025).

The sampling was done during several rounds, and the particles are thus not typical for a specific braking event but are deemed a representative sample for railway brake wear emissions. The sampling inlet is located about 3 m from the brake friction interface and is connected to the measurement equipment via a 3 m long hose with a 10 mm inner diameter. The air intake duct (315 mm diameter)

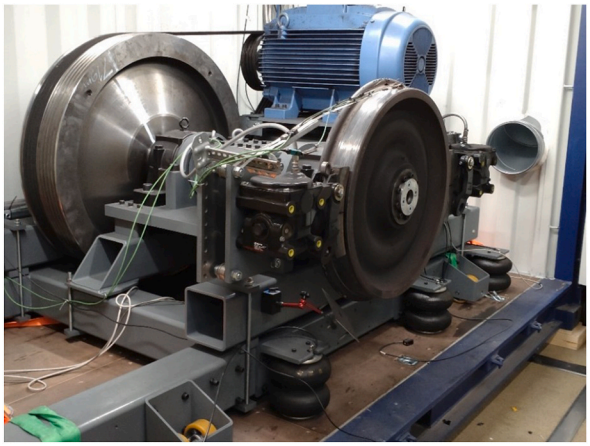

Fig. 1. Train brake test rig. Tread braking setup with steel railway wheel having brake blocks on each side, actuated by tread brake units.

operates at up to 8 m/s, while the exhaust duct of the same diameter reaches 18 m/s. The total sampling time was 7.3 h. An HR-ELPI+ (High-resolution Electrical Low-Pressure Impactor, Dekati) was used to record the time-resolved particle size distribution and a DGI (Dekati Gravimetric Impactor, Dekati) was used for collecting the particles. The DGI was operated at a high sampling flow (60 slpm) in order to collect a sufficient amount of particles. The DGI separates the aerosol into 5 different size fractions (stages), out of which 4 fractions were collected on aluminum foils. Strong enough surface forces of the PM1 BWP kept the collected PM in adhered piles on the foil removing the need for use of grease which would contaminate the chemical profile of the PM.

In this study, the size fraction from DGI stage 3 containing particles with an aerodynamic diameter of 1.1–2.7 μm was selected. The BWP were extracted from the DGI by scraping of the bare aluminum foils yielding a total mass of 129.76 mg and divided among four 15 mL Falcon tubes.

2.3. Particle suspension preparation and characterization using dynamic light scattering

A BWP stock suspension (1.5 mg/mL) was prepared using the collected BWP from DGI stage 3 suspended in MQ-water, followed by 15 min of sonication (Bransonic Ultrasonic Cleaner, Branson Ultrasonics Corporation, USA). The particle size distribution of the BWP suspension was analyzed using dynamic light scattering (DLS) (Litesizer 500, Anton Paar GmbH, Graz, Austria). The temperature of the suspension sample was kept at 37 °C during the analysis and the refractive index was set to pure water.

2.4. Cell culture

The human epithelial adenocarcinoma cell line Caco-2 (HTB-37™, ATCC, USA) was cultured in Minimum Essential Medium (MEM, Gibco, ThermoFisher Scientific, USA) supplemented with Fetal Bovine Serum (10%; Gibco, USA) and Normocin (0.2%, InvivoGen, France) at 37 °C, 5 % CO_2 and 95 % humidified air in 75 cm^2 cell culture flasks (Nunc EasYFlask, ThermoScientific, USA). The medium was changed every two to three days. The cells were passaged at approximately 80 % confluence using trypsin-EDTA (0.05%, Gibco, USA).

2.5. Cell experiments

Caco-2 cells were seeded in a 12-well plate (5000 cells/well; Costar, Corning, USA), containing glass cover slips (⌀ 12 mm, K, Sweden). The cells were cultured in MEM-FBS (10 %) Normocin (0.2 %) for 10 days. On the day of the experiment, the medium was removed, and the cells were washed with PBS (Dulbecco's phosphate-buffered saline without calcium and magnesium; Cytiva HyClone, USA). HBSS (Hank's Balanced Salt Solution, 1X, Lonza, Switzerland) was added (1950 μL) to the cell wells and to one extra well with no cells. BWP suspension was added to all wells (50 μL; final concentration in the wells: 0.0375 mg/mL), except for the HBSS control. The cells were incubated with the treatments for 2 h. The BWP suspension + HBSS control was collected, and the contents were characterized by the procedure stated in section 2.3, with a refractive index correction for saline water solution. HBSS-particle suspension from one well containing cells was collected, to measure the polydispersity using DLS. For the remaining wells, the particle suspension was aspirated. Two of the wells containing cells were washed with ammonium formate solution (0.15 M, Sigma Aldrich, USA) as preparation for the ToF-SIMS analysis. The remaining two cell wells were not washed, to check if the ammonium formate solution removes surface-bound particle suspension. The cover slips were carefully removed from the wells using sterilized tweezers and placed onto a metal plate (pre-chilled overnight at −20 °C) for snap freezing in −80 °C. The cell samples were fixed by freeze-drying overnight using a freeze dryer (Heto LyoPro 3000, Denmark) and subsequently analyzed by Scanning Electron Microscopy (SEM) and ToF-SIMS.

2.6. SEM analysis

SEM images on one region of the freeze-dried Caco-2 cells treated with ammonium formate and BWP, *i.e.* the cell sample, were captured with both secondary and backscattered electrons. The images were taken with *Quanta 200 ESEM FEG (FEI, ThermoFisher)* in low vacuum at 10.0 kV.

2.7. ToF-SIMS analysis

To investigate the chemical composition and surface interactions of the BWP and the BWP exposed cells, ToF-SIMS imaging was applied. ToF-SIMS measurements on both BWP particles and the cell sample were made.

2.7.1. ToF-SIMS setup details

ToF-SIMS analysis was performed using a TOF.SIMS 5 instrument (ION-TOF GmbH, Münster, Germany), equipped with a 30 keV Bi_3^+ cluster ion gun and a 20 keV Argon gas cluster ion source (GCIB) for precise sputtering. Some measurements of the samples were analyzed with the primary Bi_3^+ ion beam LMIG in the delayed extraction mode (DEEX) and some were analyzed with the primary ion beam in the spectroscopy mode (SM).

In **DEEX** mode a pulsed primary ion beam (Bi_3^+, 0.1 pA) with a focus of approximately 100 nm and a mass resolution of at least M/ΔM = 4000 fwhm at *m/z* 500 was used. In **SM** a pulsed primary ion beam (Bi_3^+) with a focus of approximately 1000 nm and a mass resolution of at least M/ΔM = 8000 fwhm at *m/z* 500 was used.

The software SURFACELAB (version 7.1, ION-TOF) was used to process, record, analyze and evaluate images and mass spectra. The spectra of the three separate measurements were each internally calibrated only to signals identified with high confidence which can be found in *Supplementary information (SI)* Tables ST1-ST3.

2.7.2. ToF-SIMS BWP sample preparation and SM measurement

For the BWP content analysis, 15 mg of collected particles with an aerodynamic diameter of 1.1–2.7 μm was poured onto a sheet of aluminum foil in a fume hood. A circular "SEM" carbon tape was adhered to a ToF-SIMS sample holder aluminum slab which was then turned with the adhesive side down to collect the BWP. Measurement of the BWP on carbon tape was made in positive polarity SM. Here, a 200 × 200 μm FoV area was measured by the Bi_3^+ gun at 30000 eV, 0.22 pA current to produce a 128x128 px raster in random mode per frame. 2 shots per px, 2 frames per layer together with a non-interlaced (1 s sputter, 0.5 s pause) Ar1500 GCIB sputter gun at 5000 eV and 6.08 nA current to sputter a raster crater of 500 × 500 μm to a total of 30 scans was used (15 sputter layers in total, 2 frames each).

2.7.3. ToF-SIMS cell sample SM and DEEX measurements

A measurement of the cell sample with BWP was made in positive polarity SM. A 250 × 250 μm FoV area was measured by the Bi_3^+ gun at 30000 eV, 0.22 pA current to produce a 256x256 px raster in random mode per frame. 1 shot per px, 10 frames per layer together with a non-interlaced (1 s sputter, 0.5 s pause) Ar1500 GCIB sputter gun at 5000 eV and 6.12 nA current to sputter a raster crater of 500 × 500 μm to a total of 30 scans was adopted (30 sputter layers in total, 1 frame each).

Another measurement of the cell sample with BWP was made in positive polarity DEEX mode in a different region. Here, a 250 × 250 μm FoV area was measured by the Bi_3^+ gun at 30000 eV, 0.22 pA current to produce a 512x512 px raster in random mode per frame. 1 shot per px, 10 frames per layer together with a non-interlaced (5 s sputter, 0.5 s pause) Ar1500 GCIB sputter gun at 5000 eV and 6.12 nA current to sputter a raster crater of 400 × 400 μm to a total of 20 scans was used (2 sputter layers in total, 10 frames each).

2.8. Statistical analysis

The data collected for the BWP and the two cell sample measurements were treated in a similar way. An iterative mass calibration process was performed for each measurement. Here, signals in the lower mass range (<50 m/z) that could be identified with higher certainty were first pre-calibrated on. The calibrations were then expanded by new manual identifications, made using the more accurate mass spectra with the pre-calibrations. The final mass calibrations for the measurement can be found in SI Tables ST1-ST3.

After mass calibrations and identifications, the multivariate analysis technique MCR-ALS was used on the DEEX cell sample measurement outlined in section 2.7.3. In MCR-ALS the explained variance in a dataset is maximized, imposing physically or chemically relevant constraints on the component profiles (in this case positive component profiles). The number of factors in MCR-ALS significantly impacts the results, as factors are resolved simultaneously using an iterative algorithm. This makes MCR-ALS better suited than PCA for identifying unknown mixtures and capturing the major chemical constituents' spatial distribution (J. L. S. Lee et al., 2009; Ruckebusch & Blanchet, 2013).

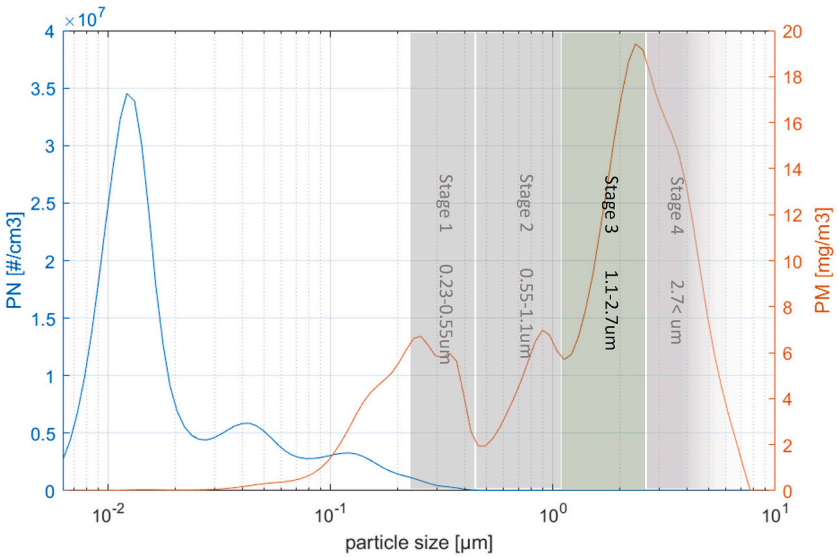

Fig. 2. HR-ELPI+ & DGI measurements. HR-ELPI + measurement where the distribution of collected mass of particle size (orange, right) and collected count of particle size (blue, left) are shown on a logarithmic x-axis of particle size by diameter (μm). An overlay of the DGI collection ranges shows how the different DGI stages compared to the HR-ELPI + measurements. (For interpretation of the references to color in this figure legend, the reader is referred to the Web version of this article.)

By screening MCR-ALS with different number of factors and settings available in the SURFACELAB 7.3 software to get the best resulting distribution separations for this data, MCR-ALS analysis was conducted using 12 factors and variance spectral scaling.

3. Results & discussion

3.1. HR-ELPI+ and DGI particle collections

The BWP was analyzed by the DGI during several rounds of brake experiments, to collect enough brake wear material. Over two weeks, tests were conducted daily apart from the first day, each lasting about 40 min. Emissions were initially dominated by coarse particles, shifting toward finer fractions as brake temperature exceeded 400 °C. For cell exposure, the selected DGI stage (1.1–2.7 μm) would be corresponding relatively coarse particles emitted early in each test. During the brake experiments the concentration of brake wear emissions and particle size distribution (PSD) also varied greatly. In Fig. 2 an average PSD is shown, using both number concentration and mass concentration. It can be observed that there are several peaks in the particle size distribution plot, especially for PM2.5, i.e. particles smaller than 2.5 μm.

3.2. Particle size characterization using DLS

To characterize the PSD, dynamic light scattering (DLS) analysis was performed on particles suspended in both ultrapure water and the cell buffer solution (HBSS) used in this study. Fig. 3 illustrates the intensity distribution of suspended particles in both matrices. In ultrapure water, the analysis showed a hydrodynamic radius of 1.2 μm with a polydispersity index (PDI) of 17.5%, suggesting a monodispersed system (Fig. 3 A). The autocorrelation function (ACF) baseline reached 1.0. Analysis of particle suspension in HBSS indicated a hydrodynamic radius of 0.5 μm with a significantly higher PDI of 239% (Fig. 3 B). This suggests a lower homogeneity in particle sizes. However, considering the ACF baseline of 9.4 for this sample, the presence of large aggregates is predicted, which can lead to a high PDI. These large particle aggregates may result from ions present in the HBSS, which could neutralize the surface charge of the particles, leading to aggregation through a coagulation mechanism.

3.3. ToF-SIMS and SEM measurements

The confluent freeze-dried Caco-2 cells treated with ammonium formate and BWP suspension were subsequently analyzed using SEM and ToF-SIMS. The freeze-dried Caco-2 cells treated with BWP suspension without the washing step with ammonium formate did not produce satisfactory contrast for cellular structures or BWP and were therefore excluded from the analysis. Therefore, it was concluded that the ammonium formate washing step was crucial for the experiments.

3.3.1. SEM imaging

SEM was used to image the topography of freeze-dried cell samples. A probable thin salt sheet covering the cells, brought to contrast through secondary electron imaging (Fig. 4 A), can be seen. Additionally, a high cell confluency was observed.

In the image generated by backscattered electrons (Fig. 4 B), the contrast shows possible agglomerated BWP on top of the confluent cells, ranging in size from 1 to 15 μm. The observed particle agglomeration is likely driven by the salt screening effect arising from the high ionic strength of the HBSS solution. This reduces electrostatic repulsion and facilitates particle clustering. As the HBSS washing was performed to remove loosely bound or unadhered particles, the remaining BWPs should be those more firmly associated with the

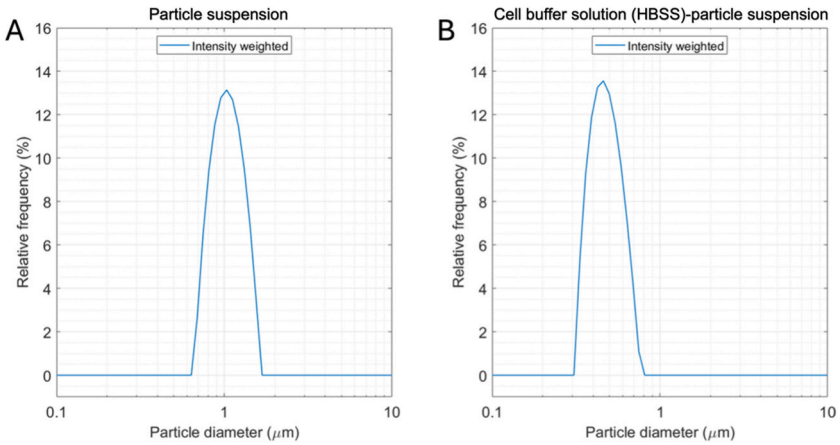

Fig. 3. Dynamic Light Scattering Analysis. Results from dynamic light scattering analysis of brake wear particle (BWP) suspension in MQ (A) before addition to Caco-2 cells and in cell buffer solution (HBSS) from Caco-2 culture exposed to BWP (B), shown as relative frequency (%) of intensity weighted by particle diameter (μm).

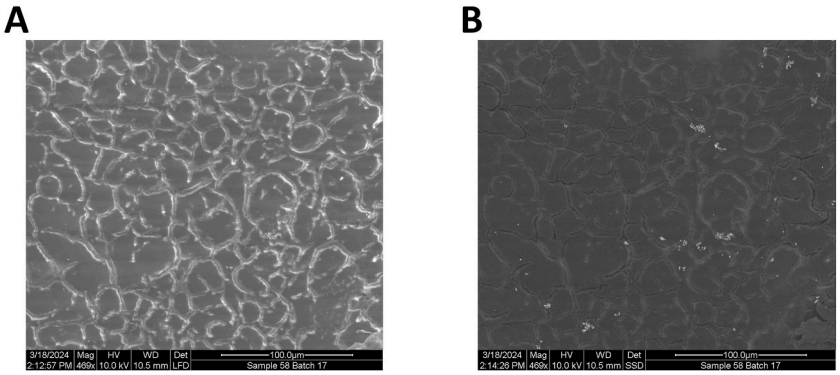

Fig. 4. SEM imaging of freeze-dried Caco-2 cell layers. SEM images of secondary electrons (A) and backscattered electrons (B) of one region of the freeze-dried Caco-2 cells treated with ammonium formate and brake wear particles.

cell surfaces. The freeze-drying process that occurred under vacuum removing water and volatiles is considered unlikely to drive particles further into the cells.

3.3.2. ToF-SIMS SM analysis of BWP

To analyze the contents of the BWP, ToF-SIMS was set to operate in SM and measurements were taken on pure BWP samples on carbon tape. 64 ion signals were manually identified post establishing a calibration and is summarized in SI Table ST4. Raw mass spectra exports of these measurements can also be viewed in SI Fig. S1.

A selection of ions relevant for BWP identification among the cells was made. Here, an exclusion of an identified C_xH_y cascade was considered to not be characteristic for the BWP content. Ion signals from sodium and potassium were additionally not considered relevant as their signals are known to register disproportionately in the ToF-SIMS analyzer. Out of the remaining signals the top 20 ions by signal area were selected and are shown in Table 1. Here, the ions for Fe^+, Mg^+, Cu^+, Ca^+, Si^+, Al^+ are recognized to be connected to the contents of the parts subdued to the stress and abrasion in the train brake particle generation rig. It is important to remember that the secondary ion phenomena do not produce detectable sample ions proportionally and thus this data cannot be used to quantify the composition of the BWP.

3.3.3. ToF-SIMS SM analysis of cells and BWP

The freeze-dried Caco-2 cells treated with ammonium formate and BWP, i.e., the cell sample, was analyzed in SM with ToF-SIMS. Post calibrations, ion images on the *m/z* of the top 20 relevant BWP ions (Table 1) were captured and can be found in SI Fig. S2. Through evaluation of these images and the assumption that the BWP would contain a significant amount of iron, it can be concluded that there are uniquely BWP deposited on the cell epithelial surface. Here, the Fe^+, FeH^+, $FeOH^+$, Cu^+, Ca^+ and Mg^+ ions are observed to have a similar distribution while Si^+ and SiH^+ distribute together differently.

Table 1
The top 20 identified BWP ions measured with ToF-SIMS. Name, ion mass (u), mass deviation (ppm), explained (%) and area. Selection sorted by signal area.

Assignment	Ion Mass (u)	Mass Deviation (ppm)	Explained (%)	Area
$SiH_7N_3^+$	77.040375	0.86168	100	187764.4
Mg^+	23.984493	−13.3685	97.67	165964.1
$C_2H_5NO^+$	59.036565	30.31188	100	165551.1
Fe^+	55.934394	−15.7357	100	164727.9
Cu^+	62.929053	17.50841	100	148547.9
$C_2H_3O^+$	43.017841	21.60932	100	146299.2
Ca^+	39.962043	−17.0964	100	112101.3
$C_2H_5O^+$	45.033491	37.77593	100	91703.2
$CaOH^+$	56.964782	8.228059	100	88143.0
$^{65}Cu^+$	64.927245	15.56413	99.62	65291.1
$C_2^{13}CH_7^+$	44.057581	28.05692	69.75	38067.1
CH_3^+	15.022927	21.38168	100	37780.8
Si^+	27.976378	−32.1508	100	29381.4
Al^+	26.98099	−17.2511	100	28993.9
$FeOH^+$	72.937133	4.736742	100	26514.4
FeH^+	56.942219	−31.1708	100	24614.7
CH_3O^+	31.017841	25.08744	100	23742.9
$^{26}Mg^+$	25.982044	−18.6649	100	21405.2
$^{25}Mg^+$	24.985288	−30.1784	95.1	18001.9
SiH^+	28.984203	−2.66681	100	13915.3

3.3.4. ToF-SIMS DEEX analysis of cells and BWP

The cell sample was analyzed in DEEX mode to produce a higher spatial resolution, but lower mass resolution data in order to assess how the identified BWP interact with the cell epithelia. Post calibrations, common ToF-SIMS ions from the phosphatidylcholine headgroup (PC) (*m/z* 184.04) (Richter et al., 2007) and the cholesterol (*m/z* 369) (Nygren et al., 2006) signals, were identified together with $Si^{+,}$ which are shown in greater detail in SI Fig. S3. Here, only the PC ion image displayed ample cell structure contrast. Through additional evaluation, a new ion of *m/z* 156.88 was observed to produce exceptionally great contrast for the cell membranes. Through an RGB ion signal image overlay these observed cell signals were combined with the signal image of Fe^{+}, shown in Fig. 5. It is possible to confirm that the BWP appear to form aggregates ranging in sizes around 1–10 μm, much like observed with SEM. By examining the signal intensity distribution of the total ion image (Fig. 5b), the PC *m/z* 184.04 and the Fe^{+} *m/z* 55.93 ion images (SI, Fig. 3e and f), it can be observed that the total and PC signal are notably lower in the regions in which the Fe^{+} provides a signal. The analysis itself does not produce accurate depth information, but observations of signal overlap can conclude that the BWP is deposited on top of the Caco-2 cells, as ions from the cells are not seen through the particle agglomerates.

3.3.5. ToF-SIMS MCR-ALS analysis of cells with BWP

The same calibrated DEEX measurement data of the cell sample was then further evaluated using the multivariate analysis method MCR-ALS. The MCR-ALS data fitting produced 12 factor distribution images displayed with the Average 2 filter, found in SI Fig. S4. The factors 3, 4, 6, 8, 11 and 12 displays good contrast and separation of the underlying distributions (see Fig. 6).

Through cross examination of the factor's spatial distributions and their respective component loadings (SI Fig. S5) it can be concluded that factor 4 (Fig. 6b) includes significant loadings from ions previously identified as Fe^{+} and FeH^{+}. Factor 3 and 12 (Fig. 6a and f) share distribution with the previously identified PC (*m/z* 184.97) and fragment *m/z* 156.88, respectively (see SI Fig. S3). Factor 11 appears to show a distribution much alike what is given contrast for in the total ion images which are mostly representative the of Na^{+} and K^{+} signal. Thus, factor 11 likely displays the distribution of the residual salt sheet with some cracks on top of the cells. Factor 6 (Fig. 6c) correlates with the signal distributions of aluminum and silicon, which both are significant loadings for the factor. Here, the Fe^{+} signal does not correlate and given the size and morphology of the structure contrasted in Factor 6 it is concluded not to be BWP. This factor displays what could be fragments left from the sample methodology and handling, since aluminum foil was used in the DGI segments for particle collection, or from the ToF-SIMS sample holder fixation slabs, yet this does only explain the occurrence of aluminum.

Through a factor distribution image overlay, the different distributions of Fig. 6 are put together to create a high contrast image, as shown in Fig. 7. The following observation can be made; confluent Caco-2 cell epithelium (green) with partially agglomerated BWP (red) scattered across its surface.

Evaluating the SEM images, BWP mass spectra and the ToF-SIMS MCR-ALS factor overlay image following can be established. The BWP agglomerate due to the salt screening effect induced using HBSS and the identified BWP among the cells are those which were not washed away in the post-exposure washing but which adhere and stay at the epithelial tissue. ToF-SIMS measures the topmost monolayers of molecules but can through simultaneous sputtering measure at increasing depths. Through observing the factor images for the cells (Fig. 6a and f) and the BWP (Fig. 6b) it can be spotted that in the places where there is particle signal there is a lower signal

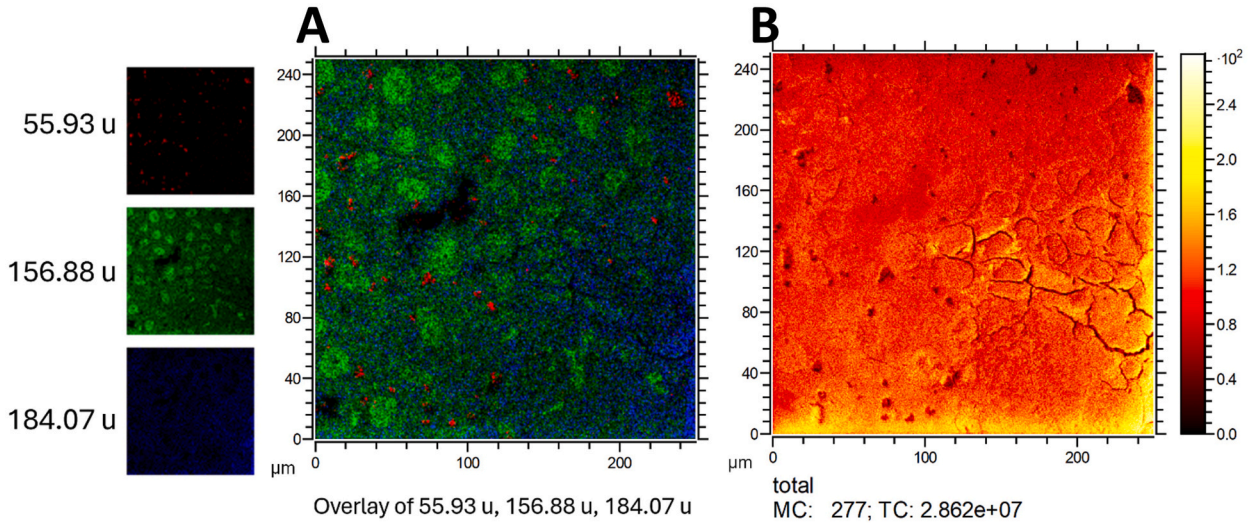

Fig. 5. ToF-SIMS ion images of ammonium formate and BWP treated Caco-2 cells. An RGB color overlay (A) of separate ion images (left) for *m/z* 55.93 (Fe^{+}) in red, *m/z* 156.88 in green and *m/z* 184.07 (phosphatidylcholine headgroup) in blue with a total ion signal image to the right (B). Measurement was done in positive polarity delayed extraction mode of a 250 × 250 μm area measured by 512x512 px random mode raster per frame together with non-interlaced GCIB sputtering. All images use the *Average 2* filter. (For interpretation of the references to color in this figure legend, the reader is referred to the Web version of this article.)

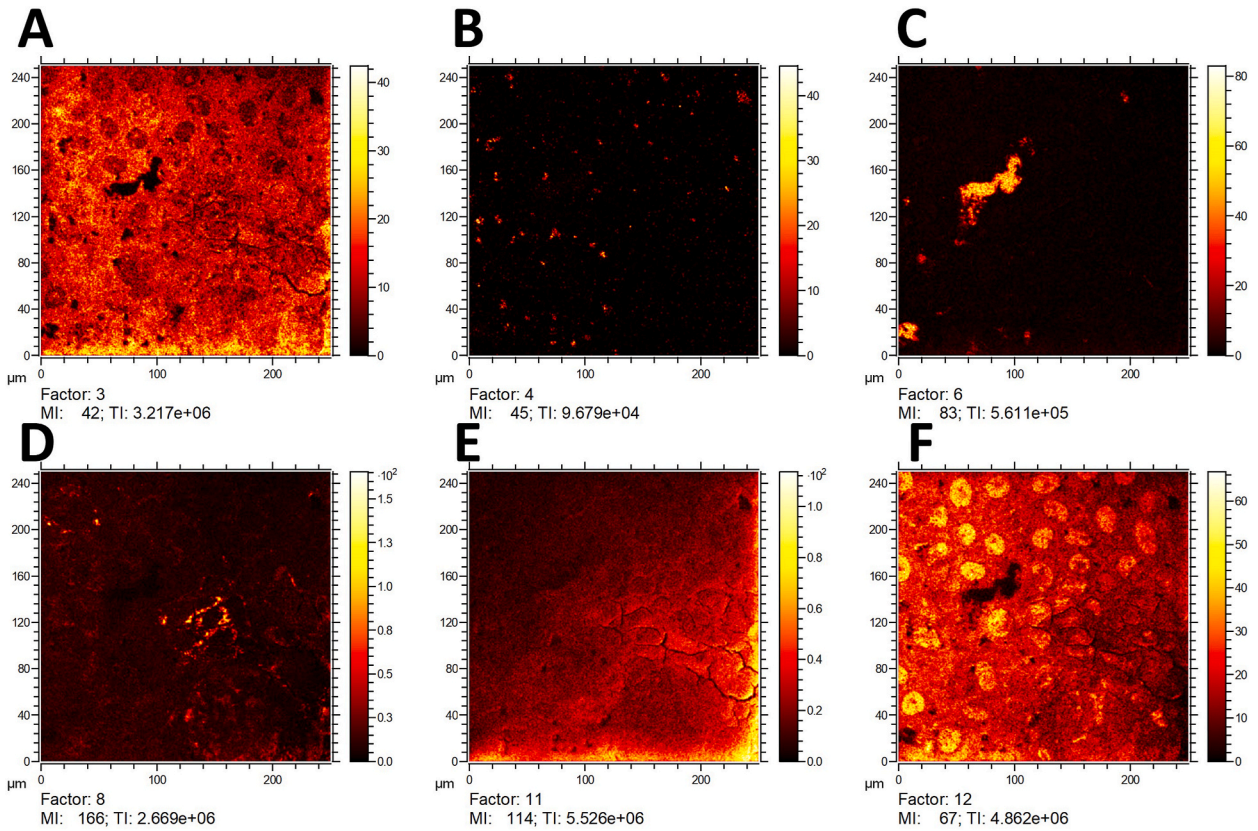

Fig. 6. ToF-SIMS MCR-ALS factor images. Selection of MCR-ALS factor images on data from measurements conducted on ammonium formate and BWP treated caco-2 cells. All images use the *Average 2* filter.

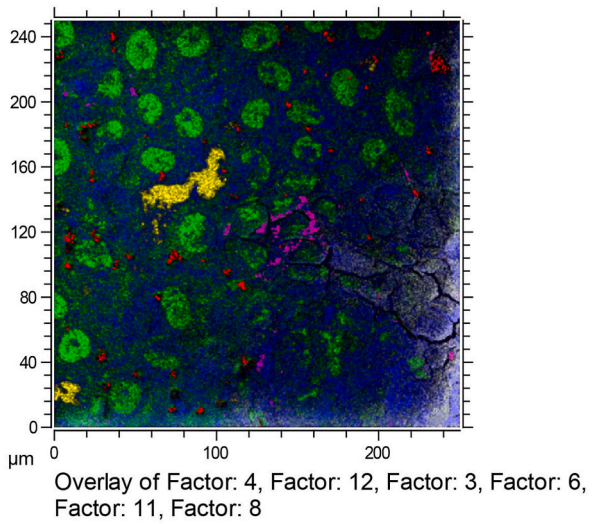

Fig. 7. ToF-SIMS MCR-ALS factor overlay image. Based on measurements conducted on ammonium formate and BWP treated Caco-2 cells. *Average 2* filtered MCR-ALS factor 4, 12, 3, 6, 11 and 8 images are overlaid and colored red, green, blue, yellow, white and magenta respectively. (For interpretation of the references to color in this figure legend, the reader is referred to the Web version of this article.)

from cell fragments. This means that the particles are on top of the cells in this measurement physically covering the cells underneath from the SIMS phenomena. The amount of sputtering used in this measurement was low and is considered to only affect the depth at a lower magnitude than the cells and particles scale. With the mass resolution of the instrument used in this study it was not possible to

resolve molecular ion fragments of higher *m/z* and with a lack of control samples, no health effects of the BWP exposure are determined by this study.

In our industrialized society with many means of transport that use brakes, the exposure to different forms of BWP is almost inevitable. The components of brakes often contain a significant fraction of iron and other minor metal modifiers which could be identified in the chemical profiles of the BWP measurements using ToF-SIMS. BWP are generated through abrasion and are likely morphologically similar across brake sources and as they are often emitted at elevated temperatures, with a significant fraction of iron, the BWP is certain to partially oxidize. Consequently, BWP from different brake sources are likely to exhibit similar chemical profiles and as other metal-rich aerosols, including BWP which are known to induce oxidative and inflammatory responses. As seen in this study, BWP chemistry and its spatial distribution can be differentiated from the cell epithelia through mass spectra analysis techniques like MCR-ALS. Previously this chemical differentiation of particles among tissue have only been shown for ToF-SIMS with nanoparticles of pure silica and zirconia. The analytical approach used here, MS imaging through ToF-SIMS provides a unique ability to simultaneously identify and image the distribution *of in situ* collected particles, metals, and organic compounds. In addition, biological processes could be monitored since lipids and metabolites can be imaged and analyzed at the same time.

In this study, BWP within the micrometer range were analyzed. Nanoparticles like gold (Singh et al., 2020), silver (Georgantzopoulou et al., 2015) and other inorganic compounds (P.-L. Lee et al., 2014), have previously demonstrated uptake in epithelial tissue. Therefore, there is an incentive to study BWP with even smaller diameters to further assess the possible cellular uptake of PM. It would also be useful to study the BWP and other particles with different analysis techniques to further establish their composition. For example, inductively coupled plasma mass spectrometry (ICP-MS) could be used to quantify their metal content.

In recent years, air-liquid-interface (ALI) cell culture models have become a popular choice to better mimic *in vivo* physiology (Baldassi et al., 2021). The use of an ALI-model with human respiratory cells could be an improvement to the model used here and further elucidate the different ways that air pollutants interact with airway cells.

While this study have not elucidated any health implications or such specific to BWP, this methodology demonstrates that it is possible to go from collection to exposure of non-animal models to analysis of more chemically complex PM. More recent ToF-SIMS instruments have a significantly greater mass resolution and slightly better spatial resolution. This method using a higher mass resolution ToF-SIMS would make molecule ion fragment identifications more precise and in the data, there should be a basis for making significant identifications of changes in biology post-exposure such as for metabolites, lipids and metals as in a mass spectrum from ToF-SIMS all are measured simultaneously with spatial distribution information all in one instrument.

3.4. Conclusions

ToF-SIMS and SEM provided detailed visual and chemical insights into the particle-cell interface. SEM images confirmed a high degree of confluency of the Caco-2 cell epithelia and a successful freeze drying and washing process, as well as deposition of agglomerated BWP on the cell surface. ToF-SIMS measurements on only BWP identified 64 ions with high confidence, of which metal ions for Fe^+, Mg^+, Cu^+, Ca^+, Si^+, Al^+ were some of the elements found. By further measurements on the cells exposed to BWP suspension and identification of BWP relevant ions on the surface, such as Fe^+, Mg^+, Cu^+, Ca^+ and how they share a similar spatial distribution, BWP presence was confirmed. DEEX measurement images with contrast of cell structures with the particles established the presence of partially agglomerated BWP particles deposited on top of the Caco-2 epithelia. Here, a previously undocumented fragment of *m/z* 156.88 was identified to show great contrast of the cellular structures, which requires continued investigation. With MCR-ALS on this data, further contrast of the different chemical distributions in the measurement data was achieved that also revealed previously unknown distributions.

The study demonstrated that ToF-SIMS, combined with MCR-ALS, is a viable option in distinguishing and characterizing *in situ* collected, chemically complex BWP interactions with epithelial cells. Current means of studying health implications of PM use many different instruments to piece together a picture of what is going on while the promise of a proper ToF-SIMS methodology could be an all-in-one, from collection to health effect method. This methodology is a great basis for such further ToF-SIMS measurements with higher mass and spatial resolution as a technique for gaining a better understanding of the mechanisms by which air pollutants affect human health, which ultimately could act as basis for more effective legislation and regulation of particle emissions.

CRediT authorship contribution statement

Robin Rydbergh: Writing – review & editing, Writing – original draft, Visualization, Methodology, Investigation, Formal analysis, Data curation. **Lisa-Marie Witte:** Writing – review & editing, Writing – original draft, Visualization, Methodology, Investigation. **Jonas Sjöblom:** Writing – original draft, Visualization, Supervision, Methodology, Investigation, Funding acquisition, Formal analysis, Data curation, Conceptualization. **Nathalie Scheers:** Writing – review & editing, Writing – original draft, Supervision, Methodology, Investigation, Funding acquisition, Conceptualization. **Amir Saeid Mohammadi:** Writing – review & editing, Writing – original draft, Formal analysis. **Eric Voortman Landström:** Writing – review & editing, Writing – original draft. **Tore V. Vernersson:** Writing – review & editing, Methodology. **Per Malmberg:** Writing – review & editing, Writing – original draft, Supervision, Resources, Investigation, Funding acquisition, Formal analysis, Data curation, Conceptualization.

Additional information

The authors declare no competing interest.

Declaration of competing interest

The authors declare that they have no known competing financial interests or personal relationships that could have appeared to influence the work reported in this paper.

Acknowledgements

This study was funded by the Health Engineering Area of Advance and Transport Area of Advance at Chalmers University of Technology.

The authors thank Patrik Wåhlin, Pavleta Knutsson and Robin Faust for their contribution to the brake wear particle collection and introduction to SEM machinery.

Appendix A. Supplementary data

Supplementary data to this article can be found online at https://doi.org/10.1016/j.jaerosci.2025.106553.

Data availability

Data will be made available on request.

References

Abbasi, S., Olander, L., Larsson, C., Olofsson, U., Jansson, A., & Sellgren, U. (2012). A field test study of airborne wear particles from a running regional train. *Proceedings of the Institution of Mechanical Engineers, Part F: Journal of Rail and Rapid Transit, 226*(1), 95–109. https://doi.org/10.1177/0954409711408774

Alfaro-Moreno, E., Torres, V., Miranda, J., Martínez, L., García-Cuellar, C., Nawrot, T. S., Vanaudenaerde, B., Hoet, P., Ramírez-López, P., Rosas, I., Nemery, B., & Osornio-Vargas, A. R. (2009). Induction of IL-6 and inhibition of IL-8 secretion in the human airway cell line Calu-3 by urban particulate matter collected with a modified method of PM sampling. *Environmental Research, 109*(5), 528–535. https://doi.org/10.1016/j.envres.2009.02.010

Ambient (outdoor) air pollution. (2022). World Health Organization. https://www.who.int/news-room/fact-sheets/detail/ambient-(outdoor)-air-quality-and-health.

Baldassi, D., Gabold, B., & Merkel, O. M. (2021). Air–Liquid interface cultures of the healthy and diseased human respiratory tract: Promises, challenges, and future directions. *Advanced NanoBiomed Research, 1*(6). https://doi.org/10.1002/anbr.202000111

Calvén, J., Ax, E., & Rådinger, M. (2020). The airway epithelium—a central player in asthma pathogenesis. *International Journal of Molecular Sciences, 21*(23), 8907. https://doi.org/10.3390/ijms21238907

EN 13979-1:2023. CEN EN 13979-1:2023 Railway applications - wheelsets and bogies - monobloc Wheels - technical approval procedure - Part 1: Forged and rolled wheels (2023). European Committee for standardization.

Darquenne, C. (2020). Deposition mechanisms. *Journal of Aerosol Medicine and Pulmonary Drug Delivery, 33*(4), 181–185. https://doi.org/10.1089/jamp.2020.29029.cd

Davies, A., & Moores, C. (2010). Structure of the respiratory system, related to function. In *The respiratory system* (pp. 11–28). Elsevier. https://doi.org/10.1016/B978-0-7020-3370-4.00002-5.

Fridell, E., Björk, A., Ferm, M., & Ekberg, A. (2011). On-board measurements of particulate matter emissions from a passenger train. *Proceedings of the Institution of Mechanical Engineers, Part F: Journal of Rail and Rapid Transit, 225*(1), 99–106. https://doi.org/10.1177/09544097JRRT407

Georgantzopoulou, A., Serchi, T., Cambier, S., Leclercq, C. C., Renaut, J., Shao, J., Kruszewski, M., Lentzen, E., Grysan, P., Eswara, S., Audinot, J.-N., Contal, S., Ziebel, J., Guignard, C., Hoffmann, L., Murk, A. J., & Gutleb, A. C. (2015). Effects of silver nanoparticles and ions on a co-culture model for the gastrointestinal epithelium. *Particle and Fibre Toxicology, 13*(1), 9. https://doi.org/10.1186/s12989-016-0117-9

Günay, M., Korkmaz, M. E., & Özmen, R. (2020). An investigation on braking systems used in railway vehicles. *Engineering Science and Technology, an International Journal, 23*(2), 421–431. https://doi.org/10.1016/j.jestch.2020.01.009

Hewitt, R. J., & Lloyd, C. M. (2021). Regulation of immune responses by the airway epithelial cell landscape. *Nature Reviews Immunology, 21*(6), 347–362. https://doi.org/10.1038/s41577-020-00477-9

Hill, W., Lim, E. L., Weeden, C. E., Lee, C., Augustine, M., Chen, K., Kuan, F.-C., Marongiu, F., Evans, E. J., Moore, D. A., Rodrigues, F. S., Pich, O., Bakker, B., Cha, H., Myers, R., van Maldegem, F., Boumelha, J., Veeriah, S., Rowan, A., … Swanton, C. (2023). Lung adenocarcinoma promotion by air pollutants. *Nature, 616*(7955), 159–167. https://doi.org/10.1038/s41586-023-05874-3

Huang, D., Xiu, G., Li, M., Hua, X., & Long, Y. (2017). Surface components of PM2.5 during clear and hazy days in Shanghai by ToF-SIMS. *Atmospheric Environment, 148*, 175–181. https://doi.org/10.1016/j.atmosenv.2016.10.036

Ivask, A., Mitchell, A. J., Malysheva, A., Voelcker, N. H., & Lombi, E. (2018). Methodologies and approaches for the analysis of cell–nanoparticle interactions. *WIREs Nanomedicine and Nanobiotechnology, 10*(3). https://doi.org/10.1002/wnan.1486

Jackson, C. (1996). Humidification in the upper respiratory tract: A physiological overview. *Intensive and Critical Care Nursing, 12*(1), 27–32. https://doi.org/10.1016/S0964-3397(96)81638-7

Jung, C.-R., Lin, Y.-T., & Hwang, B.-F. (2015). Ozone, particulate matter, and newly diagnosed Alzheimer's disease: A population-based cohort study in taiwan. *Journal of Alzheimer's Disease, 44*(2), 573–584. https://doi.org/10.3233/JAD-140855

Lee, P.-L., Chen, B.-C., Gollavelli, G., Shen, S.-Y., Yin, Y.-S., Lei, S.-L., Jhang, C.-L., Lee, W.-R., & Ling, Y.-C. (2014). Development and validation of TOF-SIMS and CLSM imaging method for cytotoxicity study of ZnO nanoparticles in HaCaT cells. *Journal of Hazardous Materials, 277*, 3–12. https://doi.org/10.1016/j.jhazmat.2014.03.046

Lee, J. L. S., Gilmore, I. S., Fletcher, I. W., & Seah, M. P. (2009). Multivariate image analysis strategies for ToF-SIMS images with topography. *Surface and Interface Analysis, 41*(8), 653–665. https://doi.org/10.1002/sia.3070

Maciejczyk, P., Chen, L. C., & Thurston, G. (2021). The role of fossil fuel combustion metals in PM2.5 air pollution health associations. *Atmosphere, 12*(Issue 9). https://doi.org/10.3390/atmos12091086. MDPI.

McConnell, R., Islam, T., Shankardass, K., Jerrett, M., Lurmann, F., Gilliland, F., Gauderman, J., Avol, E., Künzli, N., Yao, L., Peters, J., & Berhane, K. (2010). Childhood incident asthma and traffic-related air pollution at home and school. *Environmental Health Perspectives, 118*(7), 1021–1026. https://doi.org/10.1289/ehp.0901232

Mourdikoudis, S., Pallares, R. M., & Thanh, N. T. K. (2018). Characterization techniques for nanoparticles: Comparison and complementarity upon studying nanoparticle properties. *Nanoscale, 10*(27), 12871–12934. https://doi.org/10.1039/C8NR02278J

Najafinobar, N., Venkatesan, S., von Sydow, L., Klarqvist, M., Olsson, H., Zhou, X.-H., Cloonan, S. M., & Malmberg, P. (2019). ToF-SIMS mediated analysis of human lung tissue reveals increased iron deposition in COPD (GOLD IV) patients. *Scientific Reports, 9*(1), Article 10060. https://doi.org/10.1038/s41598-019-46471-7

Nygren, H., Börner, K., Malmberg, P., & Hagenhoff, B. (2006). Localization of cholesterol in rat cerebellum with imaging TOF-SIMS. *Applied Surface Science, 252*(19), 6975–6981. https://doi.org/10.1016/j.apsusc.2006.02.197

Pambianchi, E., Pecorelli, A., & Valacchi, G. (2022). Gastrointestinal tissue as a "new" target of pollution exposure. *IUBMB Life, 74*(1), 62–73. https://doi.org/10.1002/iub.2530

Particulate matter (PM) basics. (2024). United States Environmental Protection Agency. https://www.epa.gov/pm-pollution/particulate-matter-pm-basics.

Peterson, R. E., & Tyler, B. J. (2003). Surface composition of atmospheric aerosol: Individual particle characterization by TOF-SIMS. *Applied Surface Science, 203–204*, 751–756. https://doi.org/10.1016/S0169-4332(02)00812-7

Pope III, C. A. (2002). Lung cancer, cardiopulmonary mortality, and long-term exposure to fine particulate air pollution. *JAMA, 287*(9), 1132. https://doi.org/10.1001/jama.287.9.1132

Richter, K., Nygren, H., Malmberg, P., & Hagenhoff, B. (2007). Localization of fatty acids with selective chain length by imaging time-of-flight secondary ion mass spectrometry. *Microscopy Research and Technique, 70*(7), 640–647. https://doi.org/10.1002/jemt.20450

Ruckebusch, C., & Blanchet, L. (2013). Multivariate curve resolution: A review of advanced and tailored applications and challenges. *Analytica Chimica Acta, 765*, 28–36. https://doi.org/10.1016/j.aca.2012.12.028

Sarkar, C., Zhang, B., Ni, M., Kumari, S., Bauermeister, S., Gallacher, J., & Webster, C. (2019). Environmental correlates of chronic obstructive pulmonary disease in 96 779 participants from the UK biobank: A cross-sectional, observational study. *The Lancet Planetary Health, 3*(11), e478–e490. https://doi.org/10.1016/S2542-5196(19)30214-1

Singh, A. V., Jungnickel, H., Leibrock, L., Tentschert, J., Reichardt, P., Katz, A., Laux, P., & Luch, A. (2020). ToF-SIMS 3D imaging unveils important insights on the cellular microenvironment during biomineralization of gold nanostructures. *Scientific Reports, 10*(1), 261. https://doi.org/10.1038/s41598-019-57136-w

Song, S., Gao, Z., Zhang, X., Zhao, X., Chang, H., Zhang, J., Yu, Z., Huang, C., & Zhang, H. (2023). Ambient fine particulate matter and pregnancy outcomes: An umbrella review. *Environmental Research, 235*, Article 116652. https://doi.org/10.1016/j.envres.2023.116652

Tronde, A., Nordén, B., Jeppsson, A.-B., Brunmark, P., Nilsson, E., Lennernäs, H., & Bengtsson, U. H. (2003). Drug absorption from the isolated perfused rat lung–correlations with drug physicochemical properties and epithelial permeability. *Journal of Drug Targeting, 11*(1), 61–74. https://doi.org/10.1080/1061186031000086117

Upadhyay, S., Chakraborty, A., Thimraj, T. A., Baldi, M., Steneholm, A., Ganguly, K., Gerde, P., Ernstgård, L., & Palmberg, L. (2022). Establishment of repeated in vitro exposure system for evaluating pulmonary toxicity of representative criteria air pollutants using advanced bronchial mucosa models. *Toxics, 10*(6), 277. https://doi.org/10.3390/toxics10060277

Vanherle, K., Lopez-Aparicio, S., Grythe, H., Lükewille, A., Unterstaller, A., & Mayeres, I. (2021). ETC/ATNI report 5/2020: Transport non-exhaust PM-emissions. *An overview of emission estimates. relevance, trends and policies*.

Veith, L., Böttner, J., Vennemann, A., Breitenstein, D., Engelhard, C., Meijer, J., Estrela-Lopis, I., Wiemann, M., & Hagenhoff, B. (2018). Detection of ZrO2 nanoparticles in lung tissue sections by time-of-flight secondary ion mass spectrometry and ion beam microscopy. *Nanomaterials, 8*(1), 44. https://doi.org/10.3390/nano8010044

Veith, L., Vennemann, A., Breitenstein, D., Engelhard, C., Wiemann, M., & Hagenhoff, B. (2017). Detection of SiO_2 nanoparticles in lung tissue by ToF-SIMS imaging and fluorescence microscopy. *The Analyst, 142*(14), 2631–2639. https://doi.org/10.1039/C7AN00399D

Voortman Landström, E., Vernersson, T., & Lundén, R. (2024). Analysis and testing of tread braked railway wheel — effects of hot spots on wheel performance. *International Journal of Fatigue, 180*, Article 108116. https://doi.org/10.1016/j.ijfatigue.2023.108116

Voortman Landström, E., Vernersson, T., & Lundén, R. (2025). Characterisation and evaluation of global uneven heating during railway tread braking – brake rig testing and field study. *Proceedings of the Institution of Mechanical Engineers, Part F: Journal of Rail and Rapid Transit*. https://doi.org/10.1177/09544097241312943

World Health Organization. (2013). *Regional office for europe: Health effects of particulate matter: Policy implications for countries in eastern Europe*. Caucasus and central Asia. https://iris.who.int/handle/10665/344854.

Xu, Z., Li, Z., Liao, Z., Gao, S., Hua, L., Ye, X., Wang, Y., Jiang, S., Wang, N., Zhou, D., & Deng, X. (2019). PM2.5 induced pulmonary fibrosis in vivo and in vitro. *Ecotoxicology and Environmental Safety, 171*, 112–121. https://doi.org/10.1016/j.ecoenv.2018.12.061

Yang, L., Li, C., & Tang, X. (2020). The impact of PM2.5 on the host defense of respiratory system. *Frontiers in Cell and Developmental Biology, 8*. https://doi.org/10.3389/fcell.2020.00091

Zhao, C., Wang, Y., Su, Z., Pu, W., Niu, M., Song, S., Wei, L., Ding, Y., Xu, L., Tian, M., & Wang, H. (2020). Respiratory exposure to PM2.5 soluble extract disrupts mucosal barrier function and promotes the development of experimental asthma. *The Science of the Total Environment, 730*, Article 139145. https://doi.org/10.1016/j.scitotenv.2020.139145

Zhu, Y.-J., Olson, N., & Beebe, T. P. (2001). Surface chemical characterization of 2.5-μm particulates (PM2.5) from air pollution in Salt Lake City using TOF-SIMS, XPS, and FTIR. *Environmental Science & Technology, 35*(15), 3113–3121. https://doi.org/10.1021/es0019530